nature microbiology

ARTICLES

PUBLISHED: 22 FEBRUARY 2016 | ARTICLE NUMBER: 16008 | DOI: 10.1038/NMICROBIOL.2016.8

Growth control switch by a DNA-damage-inducible toxin–antitoxin system in *Caulobacter crescentus*

Clare L. Kirkpatrick[1]*, Daniel Martins[1], Peter Redder[1], Antonio Frandi[1†], Johann Mignolet[1†], Julien Bortoli Chapalay[2], Marc Chambon[2], Gerardo Turcatti[2] and Patrick H. Viollier[1]*

Bacterial toxin–antitoxin systems (TASs) are thought to respond to various stresses, often inducing growth-arrested (persistent) sub-populations of cells whose housekeeping functions are inhibited. Many such TASs induce this effect through the translation-dependent RNA cleavage (RNase) activity of their toxins, which are held in check by their cognate antitoxins in the absence of stress. However, it is not always clear whether specific mRNA targets of orthologous RNase toxins are responsible for their phenotypic effect, which has made it difficult to accurately place the multitude of TASs within cellular and adaptive regulatory networks. Here, we show that the TAS HigBA of *Caulobacter crescentus* can promote and inhibit bacterial growth dependent on the dosage of HigB, a toxin regulated by the DNA damage (SOS) repressor LexA in addition to its antitoxin HigA, and the target selectivity of HigB's mRNA cleavage activity. HigB reduced the expression of an efflux pump that is toxic to a polarity control mutant, cripples the growth of cells lacking LexA, and targets the cell cycle circuitry. Thus, TASs can have outcome switching activity in bacterial adaptive (stress) and systemic (cell cycle) networks.

Many functions have been proposed for the toxin–antitoxin systems (TASs) of bacteria, but their best-established role is in the formation of persister cells, which tolerate antibiotic exposure without being killed[1–4]. TAS mutations decrease the frequency of persisters within a population[5,6], but functional redundancy between TASs[7] and the presence of multiple TAS homologues[8] in most genomes means that it is not usually feasible to identify individual activities of TASs using forward genetic screens selecting for altered antibiotic tolerance. The HigBA TAS is widespread in bacterial chromosomes and is easily identifiable due to its unique gene order, with the toxin gene being encoded upstream of the antitoxin. With the exception of the reversed gene order, all HigBA homologues characterized so far are classical type II TASs with protein-based antitoxin (HigA) masking the toxin activity through protein–protein interaction and transcriptional repression of its own promoter, while the toxin HigB is an mRNA endonuclease of the RelE superfamily[2]. Investigation of the two HigBA homologues from *Vibrio cholerae* showed that during amino acid starvation, they induced stasis by translation-dependent mRNA cleavage[9]. The precise mechanism of HigB orthologues involves ribosome-dependent sequence-independent cleavage for *Escherichia coli* HigB[10] and at A-rich triplets (in or out of frame) for *Proteus vulgaris* HigB[11,12]. The *Mycobacterium tuberculosis* HigB paralogue cleaves tmRNA, albeit without a specific recognition sequence[13]. Thus, it has not been possible to dissect specific cleavage of mRNA(s) at the molecular level to relate individual aspects of persistence or drug tolerance of HigBA or other TASs to target transcripts *in vivo*.

The asymmetrically dividing α-proteobacterium *Caulobacter crescentus* (hereafter *Caulobacter*) encodes one HigBA TAS (and four paralogous RelBE systems[14]). Its asymmetric division programme is regulated by polarly localized proteins such as the new pole marker TipN, which drives efficient placement of the flagellar assembly factors[15,16] and the duplicated centromere region (*parS*) of the chromosome[17] to the new cell pole. Absence of TipN leads to developmental and polarity defects. Surprisingly, *tipN* mutants (Δ*tipN*) also display drastically slowed growth when exposed to the antibiotic nalidixic acid (Nal). The Nal-sensitivity of Δ*tipN* occurs despite a natural polymorphism in *gyrA* that renders gyrase insensitive to Nal. Instead, we showed that induction of the efflux pump AcrAB2-NodT underlies the Nal-sensitivity of Δ*tipN* cells[18]. AcrAB2-NodT induction occurs via the *cis*-encoded repressor TipR, which is dislodged from the *acrA* promoter (P_{acrA}) by Nal and is toxic to Δ*tipN* cells but not other polarity mutants that were tested[18].

We originally identified the *tipR-acrAB2nodT* locus through the isolation of a *himar1* transposon (*Tn*) insertion that mitigates the Nal-sensitivity of Δ*tipN* cells[18], through TipR overexpression and downregulation of AcrAB2-NodT. Here, we report two *Tn* insertions in the *higA* antitoxin gene retrieved from the same screen. We show that the HigBA TAS has a fundamental role in the cell, as a growth regulator during DNA damage stress. By probing with quinolone antibiotics with varying capacity for DNA damage (identified by small-molecule screening), we found that HigBA regulates a switch between growth promotion and inhibition, regulated by the transcription-inducing activity of these molecules and dependent on post-transcriptional cleavage of specific mRNA targets including the *acrB2* transcript and that of the master cell cycle transcriptional regulator A (*ctrA*) of *Caulobacter*.

[1]Department of Microbiology & Molecular Medicine, Institute of Genetics & Genomics in Geneva (iGE3), Faculty of Medicine/CMU, University of Geneva, Rue Michel-Servet 1, 1211 Genève 4, Switzerland. [2]Biomolecular Screening Facility, School of Life Sciences, Ecole Polytechnique Fédérale de Lausanne (EPFL), 1015 Lausanne, Switzerland. †Present addresses: Department of Fundamental Microbiology, University of Lausanne, Quartier UNIL-Sorge, CH-1015 Lausanne VD, Switzerland (A.F.). Institute of Life Sciences, Université catholique de Louvain, Place Croix du Sud 5, 1348 Louvain-La-Neuve, Belgium (J.M.).
*e-mail: patrick.viollier@unige.ch; clare.kirkpatrick@unige.ch

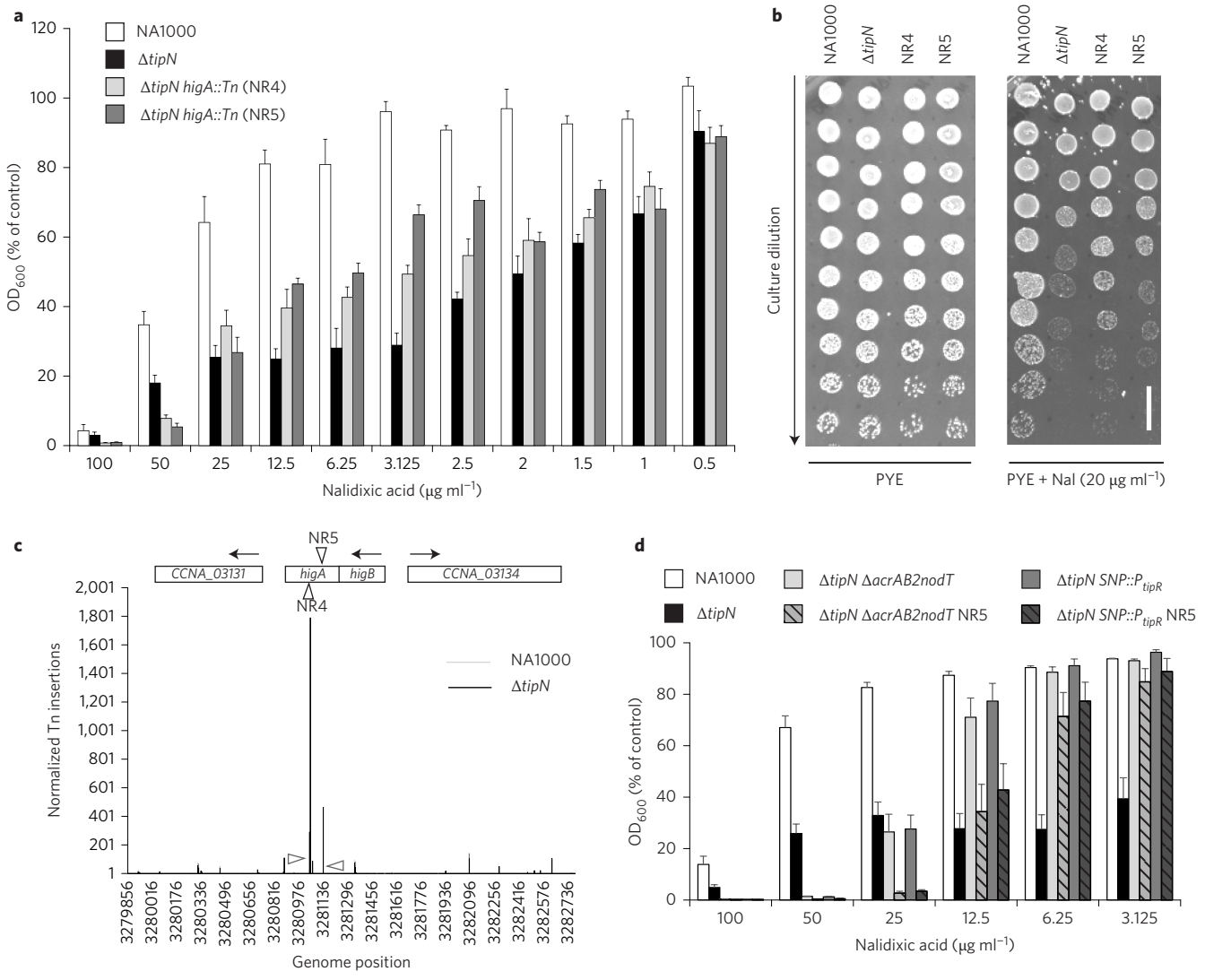

Figure 1 | Loss of function of the antitoxin HigA improves Δ*tipN* Nal tolerance. a, Growth inhibition assay of WT (NA1000), Δ*tipN* and Δ*tipN*-derived strains containing the NR4 and NR5 *higA::Tn* transposon insertions, with Nal at the indicated concentrations for 20 h at 30 °C (mean ± s.e.m., $n = 3$). **b**, Efficiency of plating assays of serially diluted mid-exponential phase cultures of the same strains as in **a** (NA1000, Δ*tipN*, Δ*tipN higA::Tn*(*NR4*) and Δ*tipN higA::Tn*(*NR5*)) on peptone yeast extract (PYE) agar with and without Nal, incubated at 30 °C for 2 days. Images are representative of three independent experiments. Scale bar, 1 cm. **c**, Tn-SEQ profiles of insertion patterns at the *higBA* locus in WT (grey) and Δ*tipN* (black) strains. This section of the genome did not contain many insertions in the WT background except for those in *higA*, which are in the same window as (and therefore masked by) those found in Δ*tipN*. The heights of these peaks in WT are indicated by grey triangles. Black triangles indicate the NR4 and NR5 transposon insertions from the Δ*tipN* Nal-resistance screen, and arrows indicate the direction of gene transcription. **d**, Growth inhibition assay of NA1000, Δ*tipN* and Δ*tipN*-derived strains (Δ*tipN* Δ*acrAB2nodT* and Δ*tipN* *SNP::*P_{tipR}) with and without the NR5 *higA::Tn* transposon insertion, incubated with Nal at the indicated concentrations for 20 h at 30 °C (mean ± s.e.m., $n = 3$).

Results

Loss of function of *higA* restores Nal resistance to Δ*tipN* cells by acting on the efflux pump AcrAB2NodT. We confirmed that the *higA::Tn* alleles in strains NR4 and NR5 [Δ*tipN higA::Tn*(*NR4*) and (*NR5*)] improved the viability and growth of Δ*tipN* cells with Nal (Fig. 1a,b). These *Tn* insertions caused loss-of-function of *higA* and did not alter Nal resistance through polar effects on downstream genes (Supplementary Fig. 1a,b). However, the upstream gene (toxin *higB*) was required to protect Δ*tipN* from Nal, as Δ*tipN* Δ*higBA* had an identical Nal resistance profile to Δ*tipN* (Supplementary Fig. 1c). Because these Nal-resistant *Tn* mutants had been obtained by direct selection on Nal, which did not indicate whether the mutagenesis was saturating, we performed transposon mutagenesis coupled to deep sequencing (Tn-SEQ)[19] to quantify the frequency of *Tn* insertions in wild type (WT) and Δ*tipN*. Insertions at the same two positions where the *Tn* insertions in NR4 and NR5 had occurred were tenfold more abundant in Δ*tipN* than in WT (Fig. 1c), showing that *higA* mutation is also favoured in a saturated screen. The mutants for Tn-SEQ were selected on Nal to eliminate the *E. coli Tn* delivery (conjugative) strain, indicating increased fitness of Δ*tipN higA::Tn* mutants compared to other Δ*tipN Tn* mutants on Nal.

To investigate whether these *higA::Tn* alleles act via *tipR-acrAB2nodT*, we conducted genetic epistasis experiments with the *higA::Tn*(*NR5*) allele and two strains in which Nal no longer induces *acrAB2nodT* expression (Δ*tipN* Δ*acrAB2-nodT* or Δ*tipN* *SNP::*P_{tipR}) to test whether *higA::Tn* further improves their growth in Nal. The *SNP::*P_{tipR} allele is a promoter-up mutation in the gene *tipR* encoding the repressor of P_{acrA} and causes downregulation (and desensitization to Nal) of AcrAB2-NodT expression[18]. Unlike the improvement of growth in Nal conferred by *higA::Tn*(*NR5*) in Δ*tipN* (Fig. 1a), *higA::Tn*(*NR5*) did not further improve the growth

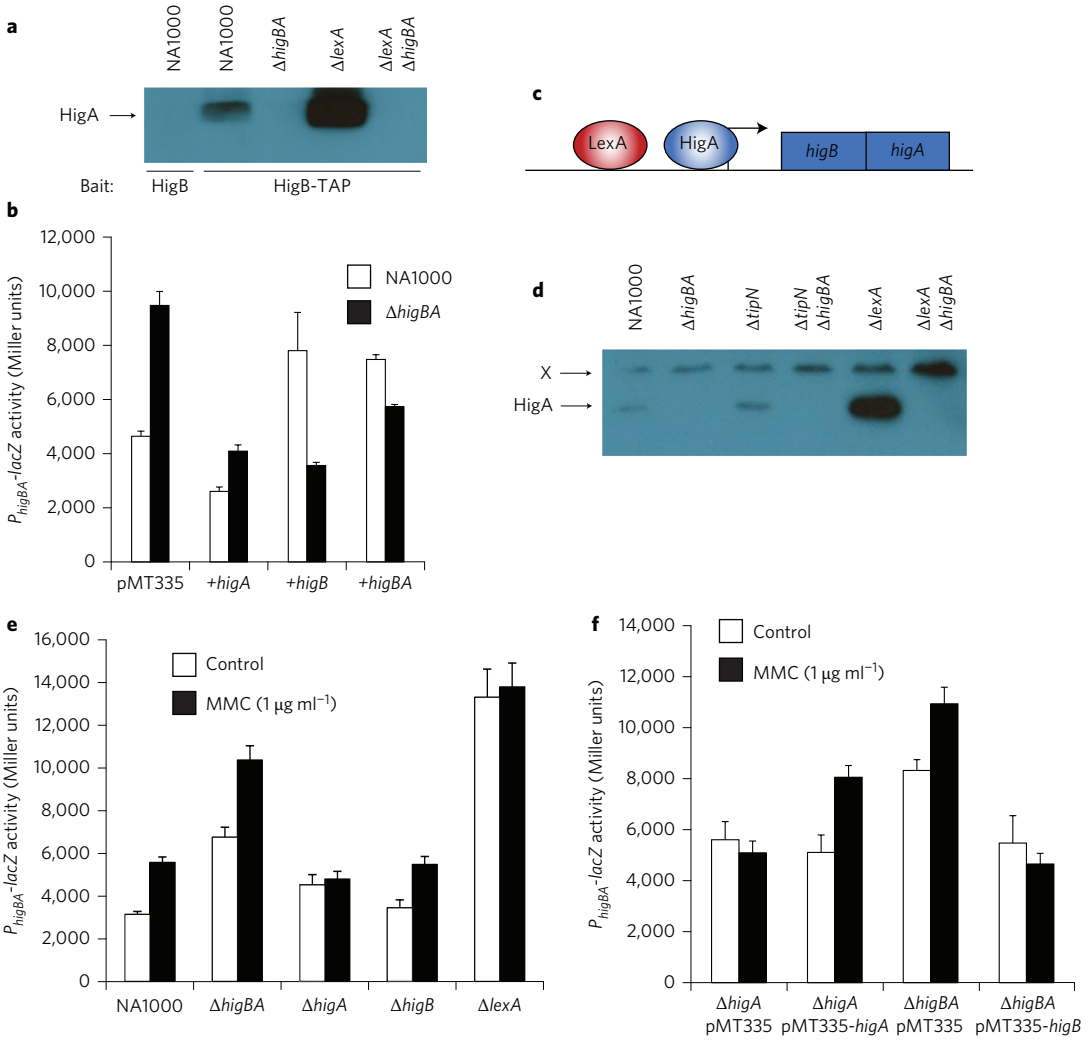

Figure 2 | HigBA is auto-regulated but also subject to hierarchically superior repression by LexA. a, Pulldown assay with HigB-TAP bait in NA1000, Δ*higBA*, Δ*lexA* and Δ*lexA* Δ*higBA* (untagged HigB in NA1000 as negative control) followed by immunoblotting for HigA. Image is representative of three independent experiments. **b**, Promoter-reporter activity of P_{higBA}-*lacZ* in NA1000 or Δ*higBA* strains complemented with empty vector pMT335, pMT335-*higA*, -*higB* or -*higBA* (mean ± s.e.m., $n = 3$). **c**, Cartoon of operon structure and regulators of *higBA*. **d**, Immunoblotting for HigA in whole-cell extracts of NA1000, Δ*higBA*, Δ*tipN*, Δ*tipN* Δ*higBA*, Δ*lexA* and Δ*lexA* Δ*higBA*. X denotes a cross-reacting protein of higher molecular mass than HigA. Image is representative of two independent experiments. **e**, Promoter-reporter activity of P_{higBA}-*lacZ* with and without 1 μg ml^{-1} MMC in NA1000, Δ*higBA*, Δ*higA*, Δ*higB* and Δ*lexA* (mean ± s.e.m., $n = 3$). **f**, Promoter-reporter activity of P_{higBA}-*lacZ* with and without 1 μg ml^{-1} MMC in Δ*higA* and Δ*higBA* strains complemented with empty vector pMT335, pMT335-*higA* or pMT335-*higB*, as indicated (mean ± s.e.m., $n = 3$). See also Supplementary Fig. 8 for full scans of immunoblots for **a** and **d**.

of Δ*tipN SNP::*P_{tipR} and Δ*tipN* Δ*acrAB2-nodT* in Nal (and even had an adverse effect at 25–12.5 μg ml^{-1} Nal) (Fig. 1d). Hence, in strains where *acrAB2-nodT* is no longer Nal-inducible, there is no further improvement in Nal-resistance upon loss of HigA function, showing that the protective effect of *higA* inactivation against Nal is most probably mediated through HigB acting on the AcrAB2-NodT efflux pump.

LexA protects against *higA* inactivation by negatively regulating the *higBA* promoter. Before characterizing the HigBA TAS, we first sought to understand why it was possible to obtain a Δ*higA* mutant at all, because mutation of *relB* or *parD* type II antitoxins is lethal[14]. Consistent with the fact that *higA*::*Tn*(*NR4*) and (*NR5*) alleles can be transduced into WT (with no Nal-tolerance phenotype, Supplementary Fig. 1d), we had no difficulty obtaining a Δ*higA* mutant that displayed similar growth kinetics and cell morphology to WT (Supplementary Fig. 2). The HigB toxin inhibited growth when induced from a plasmid (Supplementary Fig. 2a, inset) and interacted with HigA in tandem affinity purification (TAP)-based pulldown assay using HigB-TAP (Fig. 2a), confirming that HigBA is indeed a functional TAS. Overexpression of *higA* or deletion of *higBA* demonstrated negative autoregulation of the *higBA* promoter (P_{higBA}) activity typically observed for type II TASs (Fig. 2b). Consistent with previous reports[20,21] suggesting the *higBA* transcript is regulated by the SOS repressor LexA, ChIP-SEQ experiments revealed that LexA binds P_{higBA} *in vivo* (Supplementary Data Set 1). ChIP-SEQ also confirmed that the antitoxin HigA bound P_{higBA} and that this was the only locus in the genome bound by HigA and LexA (Fig. 2c; Supplementary Data Sets 1 and 2 and Supplementary Fig. 3b,c). We could not generate a Δ*lexA* Δ*higA* mutant, suggesting that this combination is synthetic lethal (probably through unrestricted activation and expression of HigB).

Confirming the regulatory role of LexA binding at P_{higBA}, we found that HigA protein levels are elevated in Δ*lexA* (Fig. 2d) and that a P_{higBA}-*lacZ* reporter is strongly upregulated in Δ*lexA* as well as in Δ*higBA* cells (Fig. 2e). Seeking exogenous inducers of *higBA* expression, we found that only the DNA-damage-inducing

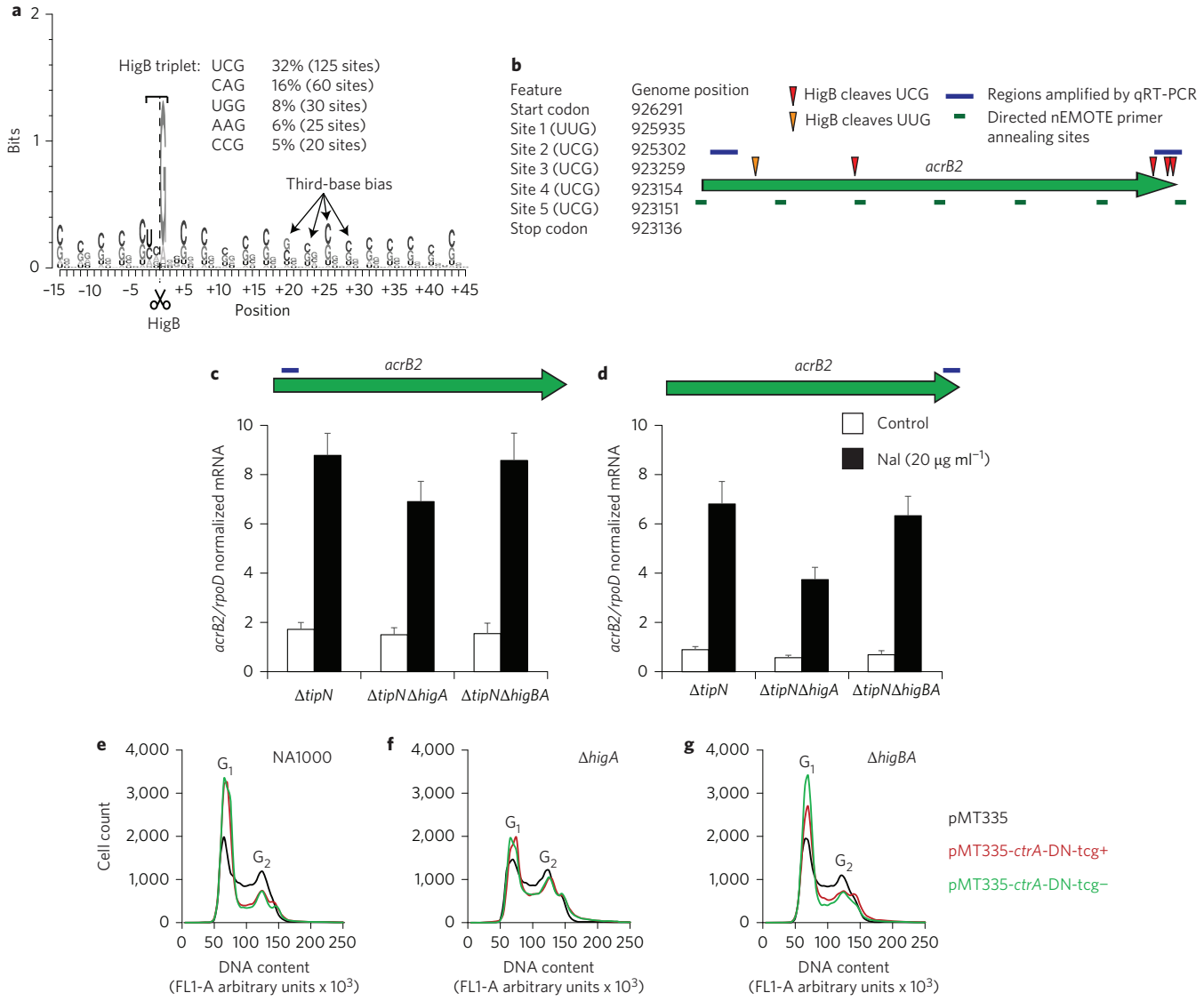

Figure 3 | HigB preferentially cleaves at UCG-Ser codons. a, Logo plot of the 386 HigB cleavage sites aligned from 15 bases upstream of the site to 45 bases downstream, with the relative % frequencies of HigB cleavage triplets indicated. The remaining 33% consists of other triplets, none of which appeared at a frequency greater than 5% of the total. **b**, Positions (from *C. crescentus* NA1000 reference genome, accession no. CP001340.1) of HigB cleavage sites in *acrB2* identified by directed nEMOTE. **c**, qRT-PCR of *acrB2* (normalized to the housekeeping gene *rpoD*) with primers amplifying at the 5′ end of the transcript in a region with no HigB cleavage sites, from RNA extracted from Δ*tipN*, Δ*tipN* Δ*higA* and Δ*tipN* Δ*higBA* cells with or without 20 μg ml^{-1} NaI for 3 h (mean ± s.e.m., $n = 3$). The difference between Δ*tipN* Δ*higA* + NaI and Δ*tipN* + NaI was not statistically significant ($P = 0.198$, two-sided unpaired *t*-test). **d**, Quantitative RT-PCR of *acrB2* (normalized to the housekeeping gene *rpoD*) with primers amplifying at the 3′ end of the transcript, encompassing two of the five HigB cleavage sites, from the same samples as in **c** (mean ± s.e.m., $n = 3$). The difference between Δ*tipN* Δ*higA* + NaI and Δ*tipN* + NaI was statistically significant ($P < 0.05$, two-sided unpaired *t*-test). **e**, Flow cytometry of NA1000 carrying empty vector pMT335, pMT335-*ctrA*-DN-tcg+ or pMT335-*ctrA*–DN-tcg–, where *ctrA*-DN signifies the coding sequence mutations D51E and C-terminal AA → DD, which cause constitutive activation of CtrA and blockage of its proteolytic removal at the $G_1 \rightarrow S$ transition, respectively. Tcg+ signifies the native serine and glutamine codon usage (that is, WT *ctrA* sequence apart from the coding mutations; native *ctrA* sequence has 6/10 Ser codons encoded by UCG, 4/4 Gln codons encoded by CAG) while tcg– signifies the sequence in which all TCG-Ser and CAG-Gln codons have been replaced by AGT and CAA respectively. Traces are the mean values of three independent experiments. **f**, Flow cytometry of Δ*higA* under the same conditions as in **e**. **g**, Flow cytometry of Δ*higBA* under the same conditions as in **e**.

compounds mitomycin C (MMC) (Fig. 2e) and the quinolone antibiotic ciprofloxacin (Supplementary Fig. 3a and Fig. 4b) induced P_{higBA} activity, while conditions known to induce other *higBA* homologues (starvation[9]), or other type II TASs of *Caulobacter* (growth phase, oxidative stresses or temperature[14]), had no effect on P_{higBA}. Hence, the viability of Δ*higA* is due to weak derepression of P_{higBA} in Δ*higA* cells with LexA preventing maximal (lethal) induction of HigB. Furthermore, a Δ*higB* deletion in Δ*lexA* cells partially improved the growth kinetics (Supplementary Fig. 2c), suggesting that HigBA is a functionally significant component of the LexA-dependent SOS response. These data provide the first (to our knowledge) example of type II TAS antitoxin-mediated autoregulation being subordinate to transcriptional regulation by a separate factor.

Surprisingly, no induction of the P_{higBA}-*lacZ* promoter-reporter construct by MMC was seen in Δ*higA*, even though there was no significant alteration of LexA occupancy at this promoter or LexA protein level between Δ*higA* and WT strains +/– MMC (Supplementary Fig. 3d,e). However, we observed a similar attenuation of P_{imuA}-*lacZ* (bound by LexA but not HigA *in vivo*) reporter activity in Δ*higA* (Supplementary Fig. 3f), suggesting non-specific

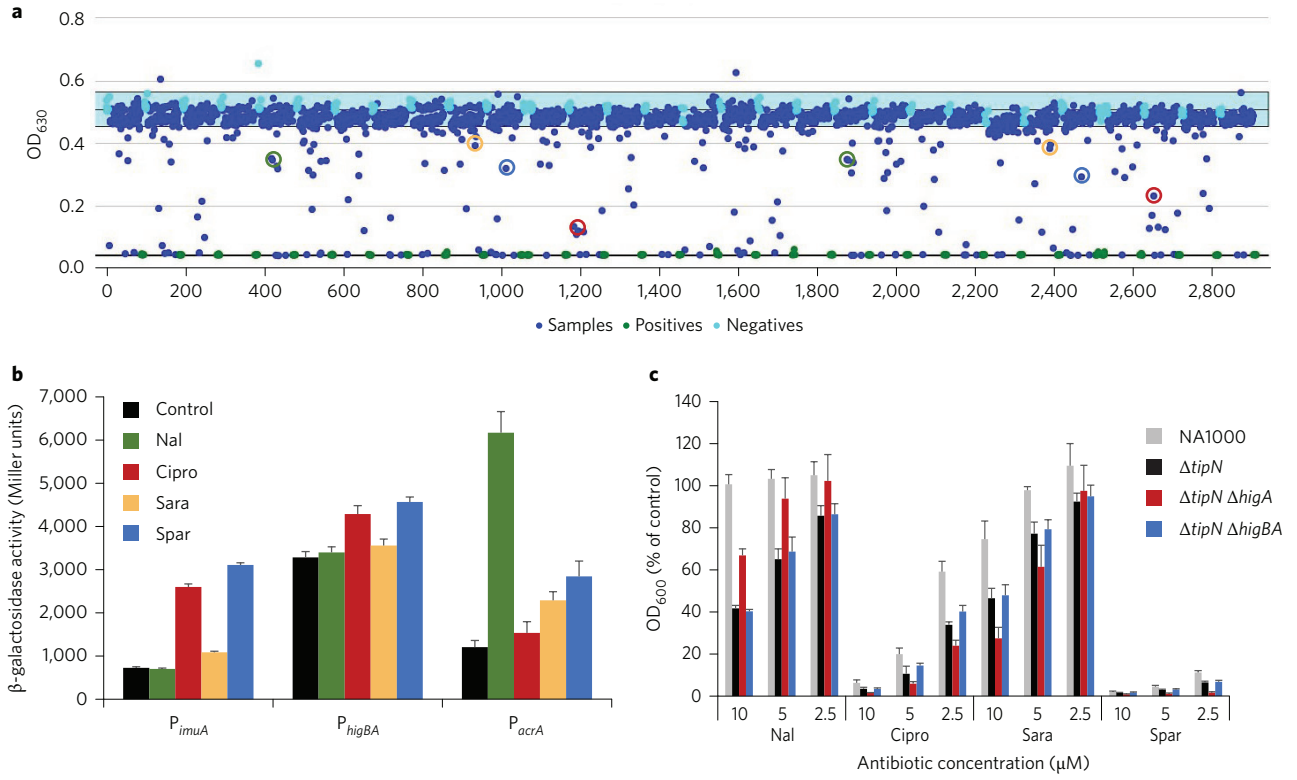

Figure 4 | Quinolone antibiotics identified from high-throughput chemical screening simultaneously activate the SOS response, *higBA* and *acrAB2nodT*. **a**, Scatter plot of the results of screening Δ*tipN* against the Prestwick Chemical Library (all library compounds at 10 μM). The vertical axis indicates growth of the cells (measured by optical density at 630 nm) and the horizontal axis denotes the number of wells. Samples (blue) correspond to wells containing library compounds, positives (green) are wells containing the positive control antibiotic chloramphenicol (2 μg ml^{-1} = 6.25 μM) and negatives (cyan) are wells containing the vehicle (DMSO at 0.1%, which does not inhibit growth). The horizontal cyan band corresponds to ± three standard deviations around the mean of the negative control wells, so anything below the coloured band corresponds to statistically significant growth inhibition. The normalized score equivalent to three standard deviations away from the mean was 0.07, but we chose the more stringent cutoff of 0.2 to eliminate the large number of low-scoring compounds identified in the Δ*tipN* screen that we considered unlikely to have a specific effect on the pathway of interest. The *Z′* score for this screen was 0.877. No overt differences were observed between this scatter plot and that obtained for the equivalent screen of WT cells (not shown), and the *Z′* score for the WT screen was 0.820. Points corresponding to selected quinolone antibiotics are indicated by circles of the following colours: nalidixic acid, green; ciprofloxacin, red; sarafloxacin, yellow; sparfloxacin, blue. **b**, Promoter-reporter activity of P_{imuA}, P_{higBA} and P_{acrA}-*lacZ* in WT with 0.1% DMSO (control) or nalidixic acid, ciprofloxacin, sarafloxacin or sparfloxacin for 3 h, all at 10 μM in DMSO, as in the chemical library (mean ± s.e.m., $n = 3$). **c**, Growth inhibition assay of NA1000, Δ*tipN*, Δ*tipN* Δ*higA* and Δ*tipN* Δ*higBA* cells with the same antibiotics as in **b**, at 10, 5 or 2.5 μM in DMSO, grown for 20 h at 30 °C, and OD_{600} values normalized to control cultures grown with DMSO alone (0.1%) (mean ± s.e.m., $n = 3$).

effects on the activity of our *lacZ* reporter. Similarly, we also saw attenuation of LacZ reporter activity in Δ*higA* when driven by the Nal-induced promoter of *acrAB2nodT* (P_{acrA}) or the xylose- and vanillate-induced promoters P_{xyl} and P_{van} (Supplementary Fig. 4). Because the loss of MMC induction of P_{higBA}-*lacZ* in Δ*higA* cells required HigB (Fig. 2f), we conclude that HigB is post-transcriptionally active against our *lacZ* reporter gene and/or the 5′ *lacZ*-fused regions of our genes of interest.

Transcriptomic 5′OH mapping of specific HigB-dependent cleavage within the toxic efflux pump *acrAB2nodT* and the cell cycle regulator *ctrA*. To test if HigB downregulates transcript levels via non-specific RNA endonuclease activity, as postulated for other HigB orthologues[9–11], we adapted the EMOTE (exact mapping of transcriptome ends[22,23]) method to detect 5′OH-ended transcripts on a genome-wide scale (Supplementary Fig. 5). Hypothesizing that HigB employs the same mechanism as the closely related RelE toxin[10,24], we mapped 5′OH ends of transcripts extracted from WT, Δ*higA* and Δ*higBA* cells to identify 5′OH RNA ends that were over-represented in Δ*higA* cells and absent from Δ*higBA*, representing HigB cleavage sites. We detected 386 non-ambiguous sites cleaved by HigB (Supplementary Data Set 3). There was a preference (87%) for cleavage at G bases, often at the third base of a UCG-serine codon, and a bias towards C or G every third base before and after the cleavage site (Fig. 3a), not observed in 386 randomly selected control sequences (Supplementary Fig. 6a). The third-base C/G bias was characteristic of *Caulobacter* protein coding sequences (Supplementary Fig. 6b). Genome-wide codon preference analysis for UCG-serine relative to other serine codons showed that HigB target transcripts were enriched for UCG-serine, as was *acrB2* (selected targets are listed in Table 1 and genome-wide UCG-Ser codon usage in Supplementary Data Set 4). Measuring the abundance of two other positive and negative control transcripts (*rsaA* and *CCNA_01138*, respectively) confirmed that for these genes, over- or under-representation of UCG-Ser correlated with decreased or increased mRNA levels in Δ*higA* relative to WT (Supplementary Fig. 6c).

Initially, *acrB2* did not appear in our set of 386 preferred HigB cleavage sites, but we hypothesized that it is weakly transcribed in the conditions (no Nal) used for RNA preparation and we probably had insufficient sequencing depth in our global analysis to detect it. Therefore, we generated a second set of non-phosphorylated EMOTE (nEMOTE) data using specific primers for the *acrB2*

Table 1 | Relative synonymous codon usage (RSCU) values for UCG-serine codons in selected HigB target mRNAs and in the *acrB2* transcript.

Gene identifier	Name	HigB target in nEMOTE?	No. of HigB sites	No. of UCG-Ser	RSCU [UCG-Ser]
CCNA_01059	*rsaA*	Yes	14	52	4.16
CCNA_00721	*groEL*	Yes	9	15	4.09
CCNA_02421	*exbB*	Yes	9	18	4.91
CCNA_03132	*rpsC*	Yes	5	5	3.75
CCNA_02037	*lon*	Yes	3	24	3.43
CCNA_02328	*gcrA*	Yes	2	11	4.4
CCNA_03130	*ctrA*	Yes	1	6	3.6
CCNA_00850	*acrB2*	Yes*	5*	44	3.94
CCNA_01138	N/A	No	0	0	0

RSCU values are an indication of how many times the codon is observed relative to the number of times it should be observed in the absence of any codon usage bias for a particular amino acid. Hence, a value of 1 indicates no apparent bias, >1 indicates that the codon occurs more frequently than expected, and <1 indicates that it occurs less frequently than expected (note that this does not take into account the preference for G/C at the third base of the codons). Supplementary Fig. 6c shows validation at the mRNA level of *rsaA* and *CCNA_01138* as positive and negative controls, respectively, and Supplementary Data Sets 3 and 4 for whole-genome/transcriptome analysis. *nEMOTE detection from sample re-analysis with *acrB2*-specific primers, rather than detection in the original global analysis.

gene on the same RNA samples. By increasing the sequencing depth in this way, we now observed five preferred HigB cleavage sites in *acrB2* (Fig. 3b). On measuring Nal-induced transcript levels of *acrB2* in Δ*tipN* Δ*higA* relative to Δ*tipN* or Δ*tipN* Δ*higBA* control strains by quantitative reverse transcription-PCR (qRT-PCR), it was reduced by approximately half when primers spanning two of the preferred cleavage sites were used, while primers amplifying from a region of the *acrB2* transcript lacking HigB sites showed a much smaller effect (Fig. 3c,d). Hence, we have validated *acrB2* as a genuine HigB target and conclude that HigB reduces the toxic induction of the efflux pump AcrAB2NodT by site-specific post-transcriptional mRNA cleavage in the *acrB2* transcript.

The appearance of *ctrA* in the set of preferred HigB targets (Supplementary Data Set 3) indicated that HigBA might affect cell cycle control via CtrA, a negative regulator of the G1 → S phase transition. CtrA activity is commensurate with the number of G1-phase cells in a population, so we analysed the distribution of G1/S/G2 cell types in WT, Δ*higA* and Δ*higBA* by flow cytometry and found that Δ*higA* had fewer cells in the G1 (motile swarmer) phase than the other two strains (Supplementary Fig. 7a) and that it had a slight motility defect that was exacerbated by ciprofloxacin (Supplementary Fig. 7b,c), suggesting that HigBA can modulate the cell cycle. To confirm that this effect is mediated by *ctrA*, we generated two versions of a CtrA (D51E)-DD mutant[25] that induces a G1 arrest in a dominant-negative manner when overexpressed, either with native serine/glutamine encoding (tcg+) or with the UCG-Ser and CAG-Gln codons converted to HigB-insensitive AGU and CAA (tcg–). Overexpression of both CtrA(D51E)-DD variants led to a G1 arrest in WT (Fig. 3e) and Δ*higBA* cells (Fig. 3g) but not in Δ*higA* (Fig. 3f), confirming that elevated HigB activity downregulates the effects of CtrA. We did not observe the expected difference between the tcg+ and tcg– variants in Δ*higA*, probably because (1) HigB's preference for UCG and CAG is not exclusive (Fig. 3a) and/or (2) HigB cleaves members of the CtrA regulon in addition to *ctrA* itself, which could mask the direct effects of *ctrA* serine/glutamine encoding on the cell cycle. Surprisingly, in Δ*higBA* cells the pMT335-*ctrA*(D51E)-DD-tcg- variant appeared to have a stronger dominant-negative effect (Fig. 3g), implying that in the absence of HigBA, other TASs may also regulate the cell cycle through *ctrA*, with an apparently stronger dependence on UCG/CAG codons than HigB. We note that these codons are the preferred recognition sequences of *E. coli* RelE[26] and that *Caulobacter* contains functional RelBE TASs[14]. In conclusion, the toxin HigB exerts post-transcriptional regulation *in vivo* on *acrB2* and *ctrA*, which affects Nal tolerance and cell cycle control, respectively.

Differential effect of HigB on synthetic toxicity induced by other quinolone antibiotics. To investigate whether *acrB2*-dependent synthetic toxicity could be elicited by other antibiotics than Nal in Δ*tipN* cells, we screened the Prestwick Chemical Library (1,280 compounds, of which 12–13% are known antibacterials; Supplementary Table 4) for molecules that could inhibit growth of Δ*tipN* but not WT in 96-well plate format (Fig. 4a). This high-throughput screening assay was highly robust, with Z' factors[27] >0.8 for both WT and Δ*tipN* screens. Of five validated inhibitory molecules, the antibiotics sarafloxacin and sparfloxacin caught our attention based on their structural similarity to Nal. We compared their activity as inducers of P_{acrA}, P_{higBA} or the SOS response (using P_{imuA} as reporter) against Nal as the P_{acrA} inducer or ciprofloxacin (Cipro) as the known SOS (but not P_{acrA}) inducer[18] (Fig. 4b). These quinolones induced P_{acrA} to a greater extent than Cipro, albeit less than Nal. However, both also induced the SOS response, sparfloxacin to a similar level as Cipro but sarafloxacin much less (50% increase over control), with sparfloxacin also inducing P_{higBA}.

We then performed growth inhibition assays to validate the high-throughput results and examine whether elevated HigB activity (in Δ*tipN* Δ*higA*) could protect against sparfloxacin and sarafloxacin (Fig. 4c). In this assay, sparfloxacin was highly inhibitory to all strains including WT (Supplementary Table 4), but we validated sarafloxacin as a genuine TipN-specific growth inhibitor. However, HigB did not protect against sarafloxacin as it did against Nal, but rather exacerbated growth inhibition. Because sarafloxacin did not induce P_{higBA} activity (Fig. 4b), this effect is unlikely to be a direct effect of increased *higBA* transcription and is probably synergistic with other effects of the SOS response, such as induction of other TASs or cell division inhibitors. This demonstrates that the toxin HigB can both protect and poison cells, depending on which specific stress the cells are under. HigB-mediated mRNA cleavage activity therefore controls a switch between growth promotion and inhibition along the structural continuum of quinolone structures (at least those tested here) as their ability to induce SOS increases (Fig. 5c).

Elevated HigB activity exacerbates loss of viability during DNA damage stress. We focused on sarafloxacin (Sara) as an intermediate stage in this continuum that is capable of induction of both the growth-inhibiting efflux pump AcrAB2NodT and of the SOS response, and used Nal, Sara and Cipro to probe the response of WT and Δ*lexA* backgrounds with deletions in *higA* and/or *higB* in terms of viability, DNA content and population cell size distribution. Consistent with our hypothesis that a Δ*lexA* Δ*higA* genotype is synthetic lethal from unrestricted HigB activity, Δ*higA* cells had progressively inhibited growth, with smaller colonies on Sara and a 2–3 log decrease in colony forming units (c.f.u.) on Cipro. Conversely, loss of HigB from Δ*lexA* improved its survival in the presence of these antibiotics (Fig. 5a). Although by microscopy Δ*lexA* Δ*higB* cells still appeared filamentous

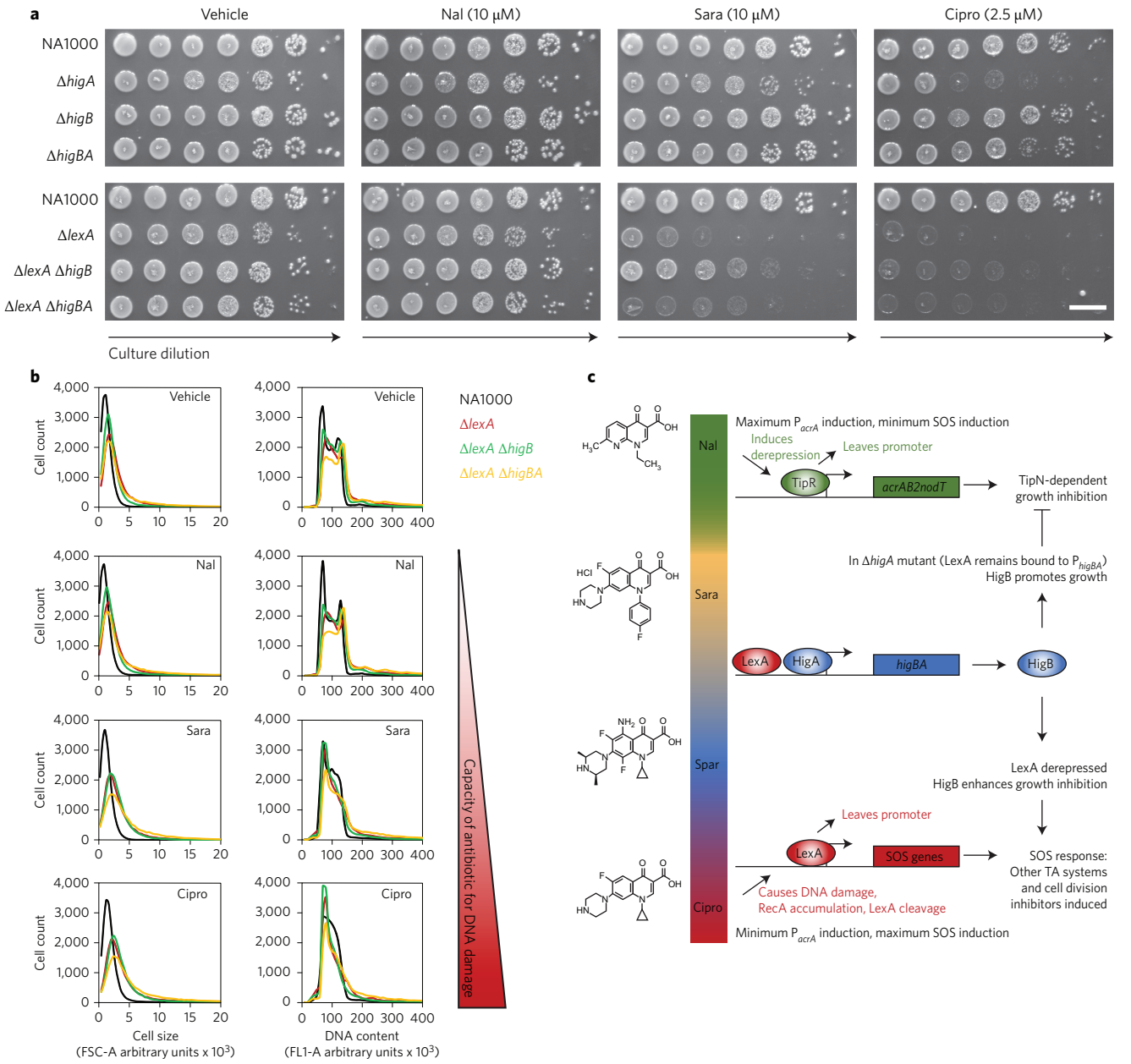

Figure 5 | HigB activity exacerbates loss of viability during the SOS response, increases cell filamentation and decreases G_1 cell accumulation in Δ*lexA* cells with constitutively activated SOS response. a, Efficiency of plating assays of serially diluted mid-exponential phase cultures of NA1000, Δ*higA*, Δ*higB*, Δ*higBA*, Δ*lexA*, Δ*lexA* Δ*higB* and Δ*lexA* Δ*higBA*, on peptone yeast extract agar with vehicle, Nal or Sara at 10 μM or Cipro at 2.5 μM (in pilot experiments, 10 μM Cipro was lethal to all strains), grown at 30 °C for three days. Images are representative of four independent experiments. Scale bar, 1 cm. **b**, Flow cytometry analysis of NA1000, Δ*lexA*, Δ*lexA* Δ*higB* and Δ*lexA* Δ*higBA* mid-exponential phase cells exposed to the same antibiotics (concentrations as in Fig. 5a) or vehicle for three hours, for forward scattering (as an indicator of cell size) and DNA content as determined by SYTOX Green staining. Traces are the average of three independent experiments. **c**, Scheme of the regulatory interplay between LexA, HigBA and AcrAB2-NodT.

(Supplementary Fig. 2d), we investigated cell size distribution by flow cytometry and found that at the population level the distribution was shifted left (that is, towards a cell size distribution intermediate between WT and Δ*lexA*) in the absence of antibiotics (Fig. 5b, left), indicating that derepressed HigB is responsible for cell death (or loss of culturability) during DNA damage stress and that it partially contributes to filamentation of Δ*lexA*.

We also measured DNA content under identical conditions and observed that increasing DNA damage capacity of the antibiotics promoted a shift towards accumulation of G1 cells in the Δ*lexA* strains, which appeared stronger in Δ*lexA* Δ*higB* cells (Fig. 5b, bottom right), suggesting that absence of HigB in Δ*lexA* cells encourages a partial G1 arrest (consistent with the HigB-dependence of the *ctrA* transcript, the reduction of G1 phase cells in Δ*higA* (Supplementary Fig. 7a) and the known role of CtrA as a negative regulator of the G1 → S transition[25]). Because loss of HigB resulted in improved antibiotic tolerance of Δ*lexA*, this partial G1 arrest seems to benefit the cells, perhaps because the bactericidal action of DNA-damaging antibiotics is more effective in a population with a higher proportion of replication-competent cells. We conclude that the differential effects of HigB on growth (and cell cycle regulation via CtrA) are tunable by the interplay between the two repressors of *higBA*, LexA and HigA (Fig. 5c).

Discussion

We report here a novel drug tolerance mechanism induced by the toxin component of the TAS HigBA mediated by downregulation, not upregulation, of *acrAB2-nodT* gene expression. Our earlier work established the genetic relationship between the polarity factor TipN and the efflux pump AcrAB2-NodT and showed that Δ*tipN* cells do not tolerate strong induction of this pump by Nal[18]. We now incorporate the TAS HigBA into this regulatory network by demonstrating that when released from HigA, the HigB toxin curbs induction of the AcrAB2-NodT system through cleavage of the *acrB2* pump component mRNA. Hence, contrary to the prevailing dogma[1], activation of this TAS directly promotes (rather than inhibits) growth through specific cleavage of one of the toxin's targets. However, this effect was specific to the context of maximum *acrAB2nodT*/minimum SOS induction that is caused by Nal. Antibiotics that induced SOS as well as *acrAB2nodT* were more inhibitory if HigB was active, suggesting a synergistic interaction between HigBA and other components of the SOS response (potentially via other LexA-regulated RNase toxins), allowing the cells to mount a precise response tailored to the nature of the stress that they are under. In the natural environment, such stress could also include chemical attack by other microorganisms. As Nal is a synthetic quinolone, it is unlikely to be the natural ligand of TipR. However, it is evident from visual inspection of the structures of the quinolone compounds employed here that maximal induction of *acrAB2nodT* expression is associated with the quinolone (Nal) with the simplest structure and that increasing complexity of the molecule is associated with decreased ability to induce the efflux pump, despite its increasing capacity for DNA damage (Fig. 5c). We note that relatively simple quinolone compounds are produced by other environmental bacteria (for example, *Pseudomonas*) as signalling molecules[28]. Thus, TipR may be a sensor for impending attack by other bacteria, and AcrAB2NodT a defence mechanism against it.

Consistent with a prominent role for HigBA in the SOS response of *Caulobacter*, we found that deleting *higB* from Δ*lexA* (which has the SOS response constitutively induced, including other TASs) led to an improvement in survival on DNA-damaging antibiotics. Conversely, deleting *higA* was impossible in Δ*lexA*, while it led to attenuation of growth and survival in Δ*higA* relative to WT exposed to the same antibiotics. Thus, in this context HigBA does not act as part of a cumulative response in concert with other TASs, but as a specific mediator of TAS-induced cell death after DNA damage. Similar activity has been postulated for other systems[29], but not dedicated to a single conserved pathway such as the SOS response. However, the increase in G1 cells seen in Δ*lexA* Δ*higB* relative to Δ*lexA* cells and the effect of HigB on dominant-negative *ctrA* suggests that HigB also exerts a specific regulatory role on the cell cycle. Loss of the mRNase activity of HigB against *ctrA* might increase CtrA protein levels to a point where the G1 → S transition is impeded. On the other hand, it may be that the effect of HigB on *ctrA* and/or other targets is most relevant *in vivo* during SOS through LexA derepression, in which case comparing nEMOTE profiles between Δ*lexA* and Δ*lexA* Δ*higB* cells could identify the preferred SOS-specific HigB targets that contribute to cell death. In sum, although we initially identified HigBA through its effect on Δ*tipN* cells exposed to Nal, we have shown that its major role in the cell is as a tuner switch that influences the cell cycle and the DNA damage response, with variable output depending on the level of transcriptional induction that is controlled by LexA and HigA.

Methods

Growth conditions. *Caulobacter* and *E. coli* strains were grown in peptone yeast extract (PYE) at 30 °C and Luria broth (LB) at 37 °C, respectively, with appropriate antibiotics. Electroporations, conjugations from *E. coli* to *Caulobacter*, and generalized transduction with ΦCr30 bacteriophage were performed as described in ref. 30. Nal and MMC stock solutions were prepared in water at 100 mg ml^{-1} and 100 μg ml^{-1}, respectively. For chemical screening follow-up experiments, stock solutions of Nal, Cipro, sarafloxacin and sparfloxacin were prepared at 10 mM in DMSO and used at 10 μM (β-galactosidase assays) or 10, 5 and 2.5 μM (growth inhibition assays) compared to 0.1% DMSO-treated controls. Details of strain and plasmid constructions are provided in the Supplementary Methods.

Growth assays. Growth inhibition assays for Nal in liquid media were performed as described in ref. 18 with the data expressed throughout as a percentage of the optical density (OD_{600}) of a control culture of each strain, including plasmid or transposon selection markers and vanillate (vanillate was used at 50 μM unless otherwise indicated) where necessary but without Nal, from three independent biological replicates. Growth inhibition assays for other quinolone antibiotics (Fig. 4) were performed identically. Growth on solid media (efficiency of plating assay) was assessed by serially (tenfold) diluting mid-exponential phase (OD_{600} = 0.5–0.6) cultures in PYE and spotting 5 μl onto PYE agar plates with antibiotics or corresponding vehicle, followed by growth at 30 °C for 48 h (Fig. 1b) or 72 h (Fig. 5), for at least three biological replicates. Growth kinetics were measured by diluting a stationary phase culture into 50 ml PYE in a conical flask to a starting OD_{600} of 0.05 and following culture density during 24 h incubation on a rotary shaker at 30 °C, for three independent biological replicates. Cell morphology was assessed by differential interference contrast (DIC) microscopy with a ×100 objective.

Tn-SEQ. Tn collections were created by conjugation from *E. coli* Tn donor into *Caulobacter* recipient strains. Approximately 100,000 kanamycin- and nalidixic-acid-resistant clones were collected for WT and Δ*tipN* strains, with the same protocol as described previously[31]. For each collection, all Tn clones were collected and DNA was extracted. Genomic DNA was used to generate barcoded ChIP-Seq libraries and submitted to Illumina HiSeq 2000 sequencing (Fasteris). Tn insertion-specific reads (50 bp long) were sequenced using the himar-Tnseq primer, generating several million reads that were mapped to the *C. crescentus* NA1000 genome (NC_011916)[32] and processed through both bowtie v0.12.9 and samtools v0.1.18 algorithms to yield a BED file encompassing the Tn insertion coordinates. We imported these files into SeqMonk v0.23.0 (www.bioinformatics.babraham.ac.uk/projects/) to assess the allocation and prevalence of Tn insertions within 5 bp windows sliding along the *C. crescentus* chromosome. Data sets were exported into Excel files and were normalized to Tn insertions per million overall reads count. The resulting file was used to assemble a histogram on which was plotted the number of Tn insertions as a function of *C. crescentus* chromosome coordinates at the *higBA* locus.

β-galactosidase assays, qChIP and ChIP-SEQ. β-galactosidase assays on strains carrying plasmid-borne transcriptional fusions of test promoters to *lacZ* were performed using the method of Miller[33] at 30 °C on early exponential phase cells (OD_{600} = 0.1–0.4) exposed to antibiotics or other inducers (as described in the main text or figure legends) for three hours, from three independent biological replicates. Chromatin immunoprecipitation experiments followed by quantitative PCR (qChIP) were performed as described previously[34]. Quantitative PCR was performed in triplicate for each ChIP or input sample, on samples from three independent biological replicates. Primers phigBA_qchip_f7/r7 were used to amplify the *higBA* promoter, and primers mipZ ChIP F1/R1 were used to amplify the *mipZ* (control) promoter. Data are expressed as ChIP to input ratios with the P_{higBA} ratio normalized to that of P_{mipZ} in each condition (so that absence of specific binding corresponds to a value of 1). ChIP-SEQ (chromatin immunoprecipitation-deep sequencing) experiments were performed and analysed as described in ref. 35.

Tandem affinity purification and immunoblotting. Tandem affinity purification (TAP) was performed as described in ref. 36. TAP extracts were prepared from cells carrying either P_{van}-*higB* or P_{van}-*higB-TAP* grown to mid-exponential phase then exposed to vanillate for 3 h. The functionality of the HigB-TAP fusion was verified by ensuring that it inhibited growth to the same extent as native HigB (both showed no visible growth after diluting 1/1,000 into PYE with vanillate followed by 20 h culture at 30 °C). Whole cell extracts were prepared from mid-exponential phase cultures normalized to culture density and resuspended in gel loading buffer. Extracts were electrophoresed on 15% (for HigA) or 12.5% (for LexA and MreB) SDS–polyacrylamide gels and transferred to polyvinylidene fluoride membranes. His6-tagged fusions of HigA and LexA were expressed in *E. coli* Rosetta and purified from the soluble fraction by Ni-NTA chromatography. Purified proteins were used to immunize rabbits for generation of antisera (Josman). Anti-HigA was diluted to 1/10,000, anti-LexA to 1/20,000 and anti-MreB[37] to 1/50,000. Immunoblots were made from at least two independent biological replicates.

Flow cytometry analysis. Cells were prepared for flow cytometry analysis by growth in 500 μM vanillate (Fig. 3) or antibiotics at the defined concentrations (Fig. 5) for 3 h to mid-exponential phase (OD_{600} of 0.3–0.5) followed by 1/10 dilution into 77% ethanol at −20 °C to fix the cells. Sample preparation and analysis was performed as in ref. 19 including RNase A digestion and staining with 0.5 μM SYTOX Green. A total of 20,000 cells were analysed per experiment for forward

scattering (FSC-A) and SYTOX Green fluorescence (FL1-A) from three independent biological replicates with data acquisition for each biological replicate performed separately. The G1 cell peak appeared at 60×10^3 to 70×10^3 FL1-A units and the G2 peak at 120×10^3 to 130×10^3 FL1-A units (as confirmed by comparison to flow cytometry of rifampicin-treated cells as in ref. 19), and the spread between the peaks corresponds to replicating (S phase) cells.

RNA extraction, qRT-PCR and nEMOTE. Cultures were grown to the mid-exponential phase and 4 ml of each was pelleted and resuspended in RNase-free TE. Cells were lysed by incubation with 2,500 U Ready-Lyse (Epicentre) at room temperature for 6 min followed by homogenization in a QiaShredder column (Qiagen). RNA was extracted from lysates with the RNEasy Mini kit (Qiagen), including an on-column DNase I digestion step, according to the manufacturer's instructions, and eluted in 40 µl RNase-free water. RNA quality was confirmed by an Agilent Bioanalyzer (Life Technologies) and the concentration was determined in a NanoDrop spectrometer. RNA (1 µg) was reverse transcribed to cDNA with the SuperScript III First-Strand Synthesis kit (Life Technologies) according to the manufacturer's instructions and used as a template for quantitative PCR, performed with triplicate measurements for each sample from three independent biological replicates. The *acrB2* transcript was amplified with primers acrB2_qrt_f1/r1 and acrB2_qrt_f2/r2, the *rsaA* transcript with primers rsaA_qrt_f1/r1, the *CCNA_01138* transcript with primers 01138_qrt_f1/r1 and the *rpoD* transcript with primers rpoD fwd/rev. Transcript abundance was quantified by the standard curve method on dilutions of NA1000 cDNA and normalized to mRNA levels of the housekeeping gene *rpoD*. RNA (15 µg) was used as template for the nEMOTE procedure (for the detailed protocol see Supplementary Methods) in two biological replicates per strain. Briefly, RNA was digested with XRN1 to remove existing mono-phosphorylated transcripts (such as would be produced by other (housekeeping) RNA degradation events), then treated with PNK to phosphorylate any 5′ OH transcript ends. The sample was then ligated to an RNA oligomer using T4 RNA ligase 1, which can only use 5′ monophosphorylated RNA as substrate. Ligation products were subjected to reverse transcription, second-strand synthesis and barcode and adaptor addition by PCR. PCR products were sequenced on an Illumina HiSeq 2500 and the sequencing reads mapped to the *C. crescentus* NA1000 genome. The data were processed as described in ref. 22 to identify the exact 5′ end of all RNA molecules in the sample. Initial data sets were generated with the EMOTEconv software package[38]. To define sites cleaved consistently by HigB, we assigned a cutoff value of two independent occurrences of a given site in the Δ*higA* and zero in the Δ*higBA* mutants to be sure that it was a non-random event and stipulated that these should be observed in both biological replicates. RNA cleavage due to other TASs could potentially be detected but should not be influenced by HigBA, and would therefore be eliminated by applying these criteria. Data processing, including application of site selection criteria and logo plot generation, was performed with a combination of R and OpenOffice Calc. Relative synonymous codon usage was analysed in Perl.

Chemical library screening. The Prestwick Chemical Library was dispensed into 96-well plates so as to have two wells (in different plates) per compound for each of the two (WT and Δ*tipN*) screens. Each plate contained eight wells negative control (DMSO), eight wells positive control (chloramphenicol) and 80 wells of library compounds and were stored at −20 °C before use. Saturated overnight cultures of WT or Δ*tipN* cells were diluted to an OD_{600} of 0.001 in 800 ml PYE. Chemical library plates were allowed to come to room temperature then centrifuged at 2,000 r.p.m. for 4 min to ensure all compounds were at the bottom of the wells. Starter culture (200 µl) was seeded into each well, lids were replaced and plates incubated at 30 °C for 48 h at which point cells in the negative control wells had reached stationary phase. Optical density (630 nm) was read and the readings compiled into a single Excel spreadsheet per screen. The person performing this experiment was blinded to the position of the library compounds in the plates. For data analysis, a score was calculated for each screen for all wells normalized to the mean of the positive control wells as the upper limit (=1) and the mean of the negative control wells as the lower limit (=0). Δ*tipN* screen-specific hits were considered as those that had a score >0.2 in the Δ*tipN* mutant but <0.2 in WT, yielding 13 compounds (including Nal), of which six (Nal and five others) passed a validation screen; the 13 compounds were seeded into new plates and the assay repeated. See Supplementary Table 4 for additional details.

Accession numbers. Source data for the ChIP-SEQ experiments (Supplementary Data Sets 1 and 2) has been deposited in the GEO database under accession no. GSE76721.

Received 26 May 2015; accepted 19 January 2016; published 22 February 2016

References

1. Cohen, N. R., Lobritz, M. A. & Collins, J. J. Microbial persistence and the road to drug resistance. *Cell Host Microbe* **13,** 632–642 (2013).
2. Gerdes, K., Christensen, S. K. & Lobner-Olesen, A. Prokaryotic toxin–antitoxin stress response loci. *Nature Rev. Microbiol.* **3,** 371–382 (2005).
3. Lewis, K. Persister cells. *Annu. Rev. Microbiol.* **64,** 357–372 (2010).
4. Schuster, C. F. & Bertram, R. Toxin–antitoxin systems are ubiquitous and versatile modulators of prokaryotic cell fate. *FEMS Microbiol. Lett.* **340,** 73–85 (2013).
5. Maisonneuve, E., Castro-Camargo, M. & Gerdes, K. (p)ppGpp controls bacterial persistence by stochastic induction of toxin–antitoxin activity. *Cell* **154,** 1140–1150 (2013).
6. Wang, X. *et al.* Antitoxin MqsA helps mediate the bacterial general stress response. *Nature Chem. Biol.* **7,** 359–366 (2011).
7. Maisonneuve, E., Shakespeare, L. J., Jorgensen, M. G. & Gerdes, K. Bacterial persistence by RNA endonucleases. *Proc. Natl Acad. Sci. USA* **108,** 13206–13211 (2011).
8. Pandey, D. P. & Gerdes, K. Toxin–antitoxin loci are highly abundant in free-living but lost from host-associated prokaryotes. *Nucleic Acids Res.* **33,** 966–976 (2005).
9. Christensen-Dalsgaard, M. & Gerdes, K. Two higBA loci in the *Vibrio cholerae* superintegron encode mRNA cleaving enzymes and can stabilize plasmids. *Mol. Microbiol.* **62,** 397–411 (2006).
10. Christensen-Dalsgaard, M., Jorgensen, M. G. & Gerdes, K. Three new RelE-homologous mRNA interferases of *Escherichia coli* differentially induced by environmental stresses. *Mol. Microbiol.* **75,** 333–348 (2010).
11. Hurley, J. M. & Woychik, N. A. Bacterial toxin HigB associates with ribosomes and mediates translation-dependent mRNA cleavage at A-rich sites. *J. Biol. Chem.* **284,** 18605–18613 (2009).
12. Schureck, M. A., Dunkle, J. A., Maehigashi, T., Miles, S. J. & Dunham, C. M. Defining the mRNA recognition signature of a bacterial toxin protein. *Proc. Natl Acad. Sci. USA* **112,** 13862–13867 (2015).
13. Schuessler, D. L. *et al.* Induced ectopic expression of HigB toxin in *Mycobacterium tuberculosis* results in growth inhibition, reduced abundance of a subset of mRNAs and cleavage of tmRNA. *Mol. Microbiol.* **90,** 195–207 (2013).
14. Fiebig, A., Rojas, C. M., Siegal-Gaskins, D. & Crosson, S. Interaction specificity, toxicity, and regulation of a paralogous set of ParE/RelE-family toxin–antitoxin systems. *Mol. Microbiol.* **77,** 236–251 (2010).
15. Huitema, E., Pritchard, S., Matteson, D., Radhakrishnan, S. K. & Viollier, P. H. Bacterial birth scar proteins mark future flagellum assembly site. *Cell* **124,** 1025–1037 (2006).
16. Lam, H., Schofield, W. B. & Jacobs-Wagner, C. A landmark protein essential for establishing and perpetuating the polarity of a bacterial cell. *Cell* **124,** 1011–1023 (2006).
17. Schofield, W. B., Lim, H. C. & Jacobs-Wagner, C. Cell cycle coordination and regulation of bacterial chromosome segregation dynamics by polarly localized proteins. *EMBO J.* **29,** 3068–3081 (2010).
18. Kirkpatrick, C. L. & Viollier, P. H. Synthetic interaction between the TipN polarity factor and an AcrAB-family efflux pump implicates cell polarity in bacterial drug resistance. *Chem. Biol.* **21,** 657–665 (2014).
19. Murray, S. M., Panis, G., Fumeaux, C., Viollier, P. H. & Howard, M. Computational and genetic reduction of a cell cycle to its simplest, primordial components. *PLoS Biol.* **11,** e1001749 (2013).
20. Da Rocha, R. P., Paquola, A. C., Marques Mdo, V., Menck, C. F. & Galhardo, R. S. Characterization of the SOS regulon of *Caulobacter crescentus*. *J. Bacteriol.* **190,** 1209–1218 (2008).
21. Modell, J. W., Kambara, T. K., Perchuk, B. S. & Laub, M. T. A DNA damage-induced, SOS-independent checkpoint regulates cell division in *Caulobacter crescentus*. *PLoS Biol.* **12,** e1001977 (2014).
22. Linder, P., Lemeille, S. & Redder, P. Transcriptome-wide analyses of 5′-ends in RNase J mutants of a gram-positive pathogen reveal a role in RNA maturation, regulation and degradation. *PLoS Genet.* **10,** e1004207 (2014).
23. Redder, P. in *RNA Remodeling Proteins* Vol. 1259 (ed. Boudvillain, M.) 69–85 (2015).
24. Neubauer, C. *et al.* The structural basis for mRNA recognition and cleavage by the ribosome-dependent endonuclease RelE. *Cell* **139,** 1084–1095 (2009).
25. Domian, I. J., Quon, K. C. & Shapiro, L. Cell type-specific phosphorylation and proteolysis of a transcriptional regulator controls the G1-to-S transition in a bacterial cell cycle. *Cell* **90,** 415–424 (1997).
26. Pedersen, K. *et al.* The bacterial toxin RelE displays codon-specific cleavage of mRNAs in the ribosomal A site. *Cell* **112,** 131–140 (2003).
27. Zhang, J. H., Chung, T. D. & Oldenburg, K. R. A simple statistical parameter for use in evaluation and validation of high throughput screening assays. *J. Biomol. Screen* **4,** 67–73 (1999).
28. Heeb, S. *et al.* Quinolones: from antibiotics to autoinducers. *FEMS Microbiol. Rev.* **35,** 247–274 (2010).
29. Engelberg-Kulka, H., Amitai, S., Kolodkin-Gal, I. & Hazan, R. Bacterial programmed cell death and multicellular behavior in bacteria. *PLoS Genet.* **2,** e135 (2006).
30. Ely, B. Genetics of *Caulobacter crescentus*. *Methods Enzymol.* **204,** 372–384 (1991).
31. Viollier, P. H. *et al.* Rapid and sequential movement of individual chromosomal loci to specific subcellular locations during bacterial DNA replication. *Proc. Natl Acad. Sci. USA* **101,** 9257–9262 (2004).
32. Marks, M. E. *et al.* The genetic basis of laboratory adaptation in *Caulobacter crescentus*. *J. Bacteriol.* **192,** 3678–3688 (2010).

33. Miller, J. H. in *Experiments in Molecular Genetics* (ed. Miller, J. H.) 352–355 (Cold Spring Harbor Laboratory Press, 1972).
34. Radhakrishnan, S. K., Thanbichler, M. & Viollier, P. H. The dynamic interplay between a cell fate determinant and a lysozyme homolog drives the asymmetric division cycle of *Caulobacter crescentus*. *Genes Dev.* **22,** 212–225 (2008).
35. Fumeaux, C. *et al.* Cell cycle transition from S-phase to G1 in *Caulobacter* is mediated by ancestral virulence regulators. *Nature Commun.* **5,** 4081 (2014).
36. Radhakrishnan, S. K., Pritchard, S. & Viollier, P. H. Coupling prokaryotic cell fate and division control with a bifunctional and oscillating oxidoreductase homolog. *Dev. Cell* **18,** 90–101 (2010).
37. White, C. L., Kitich, A. & Gober, J. W. Positioning cell wall synthetic complexes by the bacterial morphogenetic proteins MreB and MreD. *Mol. Microbiol.* **76,** 616–633 (2010).
38. Yasrebi, H. & Redder, P. EMOTE-conv: a computational pipeline to convert Exact Mapping Of Transcriptome Ends (EMOTE) data to the lists of quantified genomic positions correlated to related genomic information. *J. Appl. Bioinform. Comput. Biol.* **4**. http://dx.doi.org/10.4172/2329-9533.1000118 (2015).

Acknowledgements

This work was supported by grant no. SNF#31003A_143660 to P.H.V. and a grant from the Société Académique de Genève to C.L.K. The authors acknowledge SNF/NCCR Chemical Biology for support of the chemical screening experiments and S. Kicka, V. Trofimov, D. Moreau and H. Riezman for advice and assistance with high-throughput screening. The authors thank P. Linder for discussions and funding contributions (SNF#31003A_149228/1) for the nEMOTE experiments, G. Panis for assistance with flow cytometry data acquisition and interpretation, C. Menck for the P_{imuA}-lac290 and pNPTSΔ*lexA* plasmids, L. Théraulaz for technical assistance, H. Yasrebi for nEMOTE data tabularization and J. Prados for assistance with R programming.

Author contributions

C.L.K. and P.H.V. conceived and designed the study and wrote the manuscript. D.M. performed experiments (reported in Figs 1, 2 and Supplementary Figs 1–4) under the guidance of C.L.K. and P.H.V. P.R. designed, performed and analysed the nEMOTE experiments and wrote the corresponding sections of the manuscript. J.M. designed, performed and analysed the Tn-SEQ experiment. A.F. and J.B.C. contributed data analysis tools and analysed ChIP-SEQ and codon usage (A.F.) and high-throughput screening (J.B.C.) data. C.L.K., G.T., J.B.C. and M.C. designed the high-throughput screening experiments and C.L.K. performed these and all other experiments. M.C. and J.B.C. co-wrote the high-throughput screening section of the manuscript.

Additional information

Supplementary information is available online. Reprints and permissions information is available online at www.nature.com/reprints. Correspondence and requests for materials should be addressed to C.L.K. and P.H.V.

Competing interests

The authors declare no competing financial interests.